PROCEEDINGS OF THE 37TH U.S. ROCK MECHANICS SYMPOSIUM
VAIL/COLORADO/USA/6-9 JUNE 1999

Rock Mechanics for Industry

Edited by

Bernard Amadei
University of Colorado, Department of Civil Engineering, Boulder, Colorado, USA

Robert L. Kranz
Colorado School of Mines, Golden, Colorado, USA

Gregg A. Scott
U.S. Bureau of Reclamation, Denver, Colorado, USA

Peter H. Smeallie
American Rock Mechanics Association, Alexandria, Virginia, USA

VOLUME 2

A.A. BALKEMA / ROTTERDAM / BROOKFIELD / 1999

Rock Mechanics for Industry, Amadei, Kranz, Scott & Smeallie (eds) © 1999 Balkema, Rotterdam, ISBN 90 5809 052 3

Damage evolution and propagation paths of en-echelon cracks

R. Weinberger
Geological Survey of Israel, Jerusalem, Israel

V. Lyakhovsky & A. Agnon
Institute of Earth Sciences, Hebrew University, Givat Ram, Jerusalem, Israel

ABSTRACT: A continuum damage mechanics model simulates the stress and damage fields and the corresponding paths of pressurized en-echelon cracks. The model includes gradual strength degradation and subcritical crack growth, together with development of process zones, strain localization and brittle failure. Prior to onset of damage, the calculated stress field around the pressurized cracks is the same as that produced by linear-elastic models. After the onset of damage, localized damage zones spread out around the crack planes, and their shape is sensitive to the state of stress. The model reproduces shapes of damage lobes and geometries of crack connections that are commonly observed around en-echelon dyke segments in sandstone. Thus, the distributed damage and the crack paths may help to better estimate the state of stress acting during growth of pressurized cracks (dykes). The close kinship between dykes and artificial hydrofracturing provides an economic incentive to incorporate our results in hydraulic fracturing analyses.

1 INTRODUCTION

Distributed damage in the form of microcrack arrays profoundly affects rock strength and rock elastic coefficents (e.g. Reches & Lockner 1994, Weinberger et al. 1994, Pestman & Munster 1996, Lyakhovsky et al. 1997b) and leads to vanishing elastic moduli at large stresses immediately before failure (Lockner et al. 1992). Rock-mechanics experiments in which damage evolve indicate that fracturing cannot be described in terms of single-crack propagation and that the inelastic process zone at the crack tip has a significant size (Yukutake 1989, Reches & Lockner, 1994). The linear elastic fracture mechanics (LEFM) approach often fails to account for the distributed damage as it assumes that the size of the process zone is negligibly small. The finite-size effect of the crack process zone is often modeled by specifying a cohesive zone near the crack tip along the crack plane (Dugdale 1960, Barenblatt 1962, 1996). This approach removes the physical unrealistic crack-tip singularity prevailing in LEFM, and is useful when the crack geometry is well defined. However, experiments in most engineering and rock-like materials indicate that a slowly propagating crack is preceded by distributed damage off the crack plane (e.g. Bazant & Cedolin 1991, Lockner et al. 1991), which possibly controls the macro-crack trajectory and the growth rate (Huang et al. 1991, Chai, 1993, Zietlow & Labuz, 1998). Thus it is desirable to account explicitly for the off-plane distribution of damage in studies of crack evolution.

In accordance with laboratory experiments, rheological models of fracturing should include subcritical crack growth, material degradation due to increasing crack concentration, macroscopic brittle failure, post-failure deformation, and healing. Continuum damage mechanics (CDM) uses irreversible thermodynamics to quantitatively account for the above deformational aspects (Kachanov 1994). Our model uses the balance equations of energy and entropy to establish a thermodynamical foundation for a rheological model under CDM (Lyakhovsky & Myasnikov 1985, Lyakhovsky et al. 1993, 1997a). The present CDM model describes the variations of elastic moduli and Poisson's ratio by a scalar damage intensity, α, that is scaled properly with the ratio of strain invariants. Lyakhovsky et al. (1997a,b) develop the model further, and constrain the final model parameters by comparing theoretical predictions with various laboratory results.

The present study applies the damage model to investigate the propagation paths, connections, and damage distribution associated with en-echelon pressurized cracks. These cracks are abundant in a variety of engineering and geological environments, and occur at length scales of millimeters to kilometers. Likewise, dykes, particularly near their peripheries, are composed of arrays of en echelon segments. For these cracks, dilation is driven by a

combination of host-rock extension and fluid pressure acting on the crack walls (Pollard et al. 1975, Nicholson & Pollard 1985). The geometry of such arrays and their associated rock deformation features are attractive subjects for structural analysis, assisting to infer the stress field acting during the arrays formation (Cruikshank et al. 1991 and references therein). In this contribution, we outline the basics of our model and compare the results to those obtained using LEFM modeling. We then examine the off-plane damage evolution for different initial geometries and states of stress. To test the applicability of the proposed model we compare the model results to observed patterns of rock deformation associated with en-echelon dyke segments in Makhtesh Ramon, Israel. The state of stress accompanying dyke emplacement is then constrained.

2 METHOD

2.1 *Damage model*

To simulate micro-cracking using continuum mechanics, it is assumed that the free energy F of the material is a function of the temperature T, elastic strains ε_{ij}, and the damage intensity α

$$F = F(T, \varepsilon_{ij}, \alpha) \tag{1}$$

The damage intensity is a non-dimensional intensive variable representing the relative density of cracks and other flaws in a laboratory specimen. Assuming that dissipation by thermal, viscous, and damage processes are independent to first order, each process contributes separately to entropy production. In the context of damage, the condition of positive entropy production is stated by the following equation (Lyakhovsky et al. 1993)

$$\frac{d\alpha}{dt} = -c\frac{\partial F}{\partial \alpha} \tag{2}$$

where c is a non-negative function of the temperature, confining pressure, and damage. The function c characterizes the temporal rate of the damage process, and in our case is as a step function, with constant values for weakening and healing. We assume that the rate of healing is significantly lower than the rate of weakening and its effect is negligibly small. For the purpose of modeling, Equation 2 is applied together with a set of equations describing how the elastic moduli depend on the damage intensity α (Agnon & Lyakhovsky, 1995) and with a criterion for the onset of damage evolution. In a convenient initial reference state, the material is crack-free and behaves in a linear-elastic fashion. Damage occurs when the modified internal friction ξ,

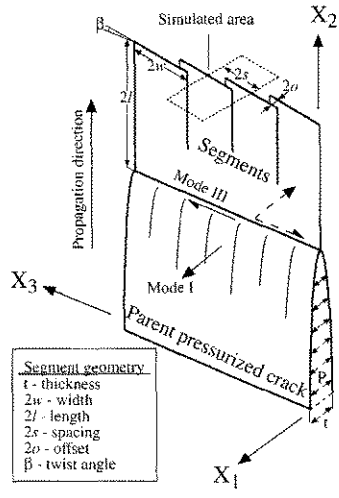

Figure 1. Schematic illustration of pressurized crack (dyke) propagation paths under mixed-mode loading.

$$\xi = \frac{I_1}{\sqrt{I_2}} \tag{3}$$

exceeds its critical value, ξ_0, where $I_1 = \varepsilon_{ii}$ and $I_2 = \varepsilon_{ij}\varepsilon_{ij}$ are invariants of the strain tensor ε_{ij} (summation convention is implied). High shear strain relative to compaction ($0>\xi>\xi_0$) or extension ($\xi>0>\xi_0$) leads to degradation, while high compaction under confining pressure ($\xi<\xi_0$) leads to healing of the material.

Following these assumptions Equation 2 may be rewritten as

$$\frac{d\alpha}{dt} = c_d I_2(\xi - \xi_0) \tag{4}$$

The positive coefficient c_d is equivalent to c in Equation 2. It is scaled to the elastic moduli and describes the rate of damage evolution for a given deformation. Thus, $1/c_d$ represents the only time scale involved in the present simulations. Current estimates of c_d values from experiments of fracturing of various rock types are between 0.5 to 5 sec^{-1} (Lyakhovsky et al. 1997a). Under shallow crustal conditions, the rate of healing is significantly smaller than these values. We model that by setting $c_d=0$ for $\xi<\xi_0$. Therefore, as long as $\xi<\xi_0$ the damage is frozen, healing does not take place, and the strain energy is fully conserved. Once ξ exceeds ξ_0, distributed damage starts to increase according to Equation 4 and grows up to its critical level. The critical level marks the onset of elastic instability and failure of the damaged region.

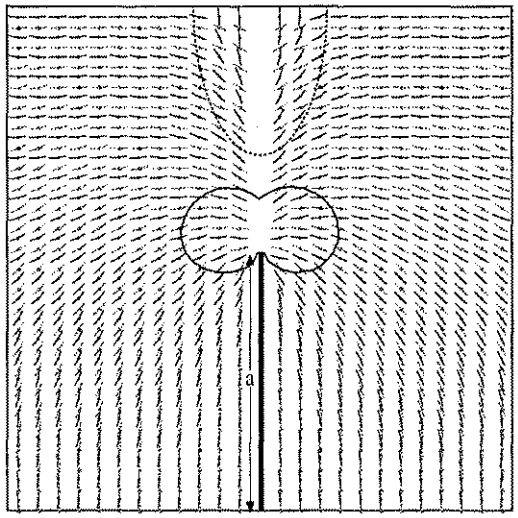

Figure 2. Tics of maximum principal (tensile) stress computed by the CDM model (broken tics) and by a boundary element model (solid tics). Solid contour defines the area of stress amplification, where stress exceeds the internal pressure. Broken contour defines the area where the stress field is approximately isotropic.

2.2 *Model setup and boundary conditions*

Propagation of en-echelon pressurized cracks is simulated under varying applied stresses, assuming that the cracks have extended far enough to be outside the influence of the parent crack (but still retain their initial twist angle β, see Figure 1). The applied stress is conveniently varied by changing the rotation angle ψ and calculating the stress ratio R (Abelson & Agnon, 1997):

$$R = \frac{\sin 2\psi}{(\frac{1}{2} - \nu)\tan 2\beta} - \cos 2\psi \qquad (5)$$

where ν is the Poisson's ratio, which is kept constant at 0.25. High values of R are related to high internal pressure p and low differential stress $\sigma_1{}^r$-$\sigma_3{}^r$, where $\sigma_1{}^r$ and $\sigma_3{}^r$ are the maximum and minimum remote principal tensile stress, respectively (tensile stress is positive). A similar applied stress state was applied by Pollard et al. (1982) and Abelson & Agnon (1997) for analyzing en echelon dilatant crack propagation in linear elastic material.

The stress and damage fields are computed in a 2D area assuming a plane strain condition. The internal fluid pressure and the remote stress produce a non-uniform elastic deformation around the cracks that is calculated using the "FLAC" algorithm (Cundall 1988, Poliakov et al. 1993). To simulate propagation of pressurized cracks, initial notches, or highly damaged regions subjected to uniform internal pressure are placed in the damage-free material. The input of the model consists of the elastic moduli of the host-rock properties, fluid pressure, damage rate coefficient (c_d), and boundary conditions that correspond to the remote stresses. For a given pair of (ψ, R) and pure shear, the principal axes of the remote stress are rotated by an angle (ψ-β) about an axis perpendicular to the simulated area such that the components of the applied stress field are resolved along the boundaries.

To test the initial conditions, the elastic strain distribution in the damage-free material corresponding to the remote stresses is calculated. The boundary conditions are mirror conditions for the top and bottom sides, and fix displacements along the left and right sides. The evolving damage modifies the effective elastic properties of the material around the notches, leading to local destruction of one or several elements of the host rock. Similar properties of the material are represented by contours of equal α intensities termed "isodamage" lines.

We assume that the process of pressurized crack propagation is quasi-static (Meriaux et al., in press). A complete analysis of the crack propagation velocity requires a simultaneous solution of the coupled equations governing host-rock deformation and fluid flow (Lister & Kerr 1991, Rubin 1993) and has not been attempted in the present study. Instead, it is assumed that propagation proceeds very slowly, and that the destroyed element is immediately filled with fluid of constant pressure, assuming an infinitely large fluid source. This algorithm allows us to simulate the geometry of the propagating en-echelon cracks, coalescing of adjacent cracks, and evolution of distributed damage around them.

3 RESULTS

3.1 *Stress field prior to and after onset of damage*

The stress field around a pressurized crack was computed by our damage model and compared with a boundary element model (Crouch & Starfield 1983). A pressurized crack that was vertically placed in the middle-bottom of the simulated area (black region in Figure 2) is composed of a highly damaged (α=1) column with a uniform internal pressure of 5 MPa. Figure 2a shows the trajectories of maximum tensile stress computed by our model and by the boundary element model for a pressurized crack in an infinite body. The grids of the two models are shifted with respect to each other by a half-element along the y axis, such that small differences between the trajectory maps can be easily detected. In the contoured region, where stresses exceeded the internal pressure because of the stress concentration, there is excellent agreement between the trajectories

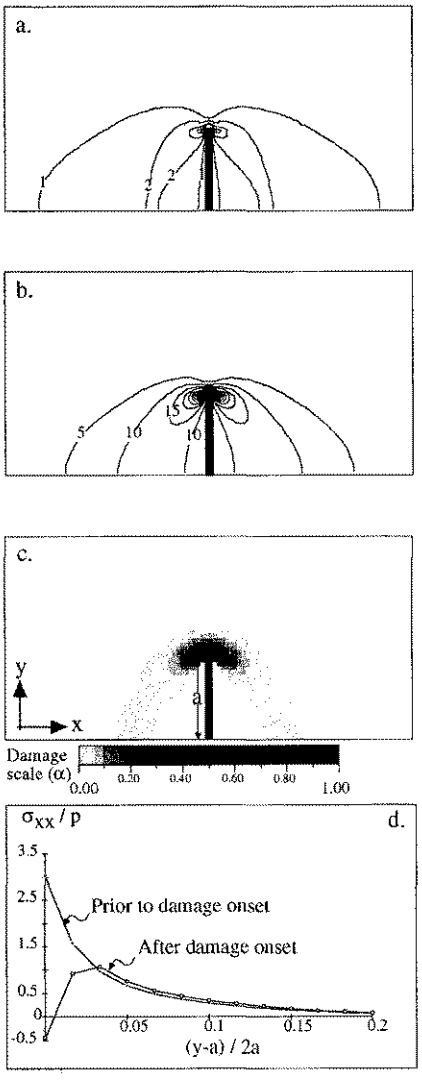

Figure 3. (a) Contours that follow Tresca Criterion prior to onset of damage. (b) Contours that follow Von-Mises Criterion prior to the onset of damage. Labels in are in MPa (c) Model distributed damage around a pressurized isolated crack immediately prior to propagation. (d) Comparison between the changes in the horizontal normalized stress σ_{xx} along the plane of an isolated (element-built) crack in a damage-free material (solid circles) and in a damaged material (empty circles) immediately prior to propagation.

of the two maps. Outside this region, the trajectories also agreed but this is less important because the stress magnitudes are low and decrease to zero. A significant deviation is observed in the region in front of the crack, contoured by the broken line. Here stresses are very close to isotropic (Jaeger & Cook 1979), and the orientation of the principal stresses is poorly defined. The similarity between our model and the boundary element model indicates that our CDM numerical model correctly calculates the stress field at the initial stage, prior to the onset of distributed damage.

To evaluate the tendency for deformation in the elastic material, it is useful to examine contours along which Tresca or Von-Mises criteria are exceeded (Collins 1993). These are shown in Figures 3a,b, respectively, which each show two sets of oval contours arranged symmetrically around the crack; the contour labels increase in magnitude as the contours decrease in size. This suggests that deformation concentrates on both sides of the crack. However, these and other criteria (Collins 1993) are not intended to describe any type of temporal material degradation or crack propagation, as the damage model is. In the damage model, the evolving damage is mostly localized to either side of the crack within two lobe-like regions (Fig. 3c), which are geometrically very similar to these shown in Figures 3a,b. The increasing damage produces strain-softening of the damaged regions, followed by non-linear response of the material in those regions, which allows the slow crack propagation. The evolving damage eliminates the physical unrealistic stress singularity at the crack tip, as clearly demonstrated by the stress profile along the crack plane (Fig. 3d). Instead of the stress amplification at the crack tip, relative magnitude of the stress components decreases to -0.5. Outside the active process zone around the crack tip, stress is the same as that obtained by the linear elastic model. This behavior of our model is similar to that prescribed by the Barenblatt model (Barenblatt 1962).

3.2 *Damage evolution around two en-echelon pressurized cracks*

The model considers propagation of two en echelon cracks toward each other with β=5 and initial crack wide w/5, where w is the cracks' final wide (Fig. 1). The cracks are subjected to a uniform internal pressure (p=5 MPa), zero remote differential stress, and zero confining pressure (Fig. 4a). At the initial stage, before the onset of crack propagation, a pair of localized damage lobes spread out symmetrically around the crack planes (Fig. 4b). At this stage, the interaction between cracks is negligible and, thus, the shape and intensity of the damage zones are similar to damage distribution near an isolated pressurized crack. Similar to mode I cracks, the cracks start to propagate in their own plane (Fig. 4c), and, simultaneously, the distributed damage develops into "lobes" of intense damage with their long axis obliquely oriented to the plane of the cracks. Continued propagation of the cracks enlarges these lobes and the intensity of the damage increases in a self-similar manner (compare Fig. 4b and Fig. 4c).

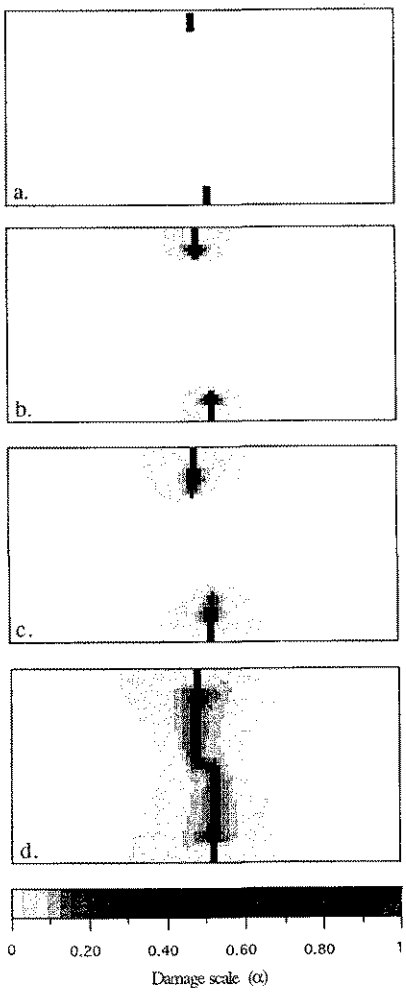

Figure 4. Sequence of mutual segment propagation and the evolution of damage.

When the wide to spacing ratio *w/s* approaches 0.8, the cracks start to interact mechanically, imposing shear stresses upon each other and enhancing damage accumulation mostly in the region between them. The direction of propagation deviates from that of in-plane, and the stress ratio increases dramatically until the cracks overlap at *w/s*=1.1. These stresses increase the differential stress, until a continuous (connected) configuration is achieved, beyond which point the simulation ceased. The stress drop at the time of crack connection implies that a final failure of the host material surrounding the cracks occurs during this stage. Subsequently, intruding fluid connected between the cracks and contributed to the final stabilization of the cracked configuration (Fig. 4d).

The style of crack interaction, their connection and shape of their damage zones significantly depend on the remote stress and confining pressure. Figure 5 summarizes variations in the shape of the distributed damage as a function of the stress state corresponding to the pair (ψ, R).

En-echelon cracks may be continuous or discontinuous in plan view depending on the state of stress prevailing during their propagation. This is illustrated for two cracks propagated under a uniform internal pressure of 10 MPa and an effective lithostatic pressure of 5 MPa (Fig. 6a). In this simulation, the effective lithostatic pressure significantly reduces the distribution and intensity of damage compared to simulations with a similar driving pressure but zero effective lithostatic pressure. This is because effective pressure inhibits material failure. Nevertheless, the bridge zone between the en-echelon cracks fails and the cracks connect, forming a continuous stable configuration. Simulations in which the magnitude of the right lateral shear stress is higher than that predict by the pair (ψ, R) produced out-of-plane distribution of damage and propagation, resulting in a discontinuity in plan view (Fig. 6b). Thus, discontinuous cracks are more likely to result from high magnitudes of shear stress while forming.

4 DISCUSSION

The model results indicate that different distribution and intensity of damage around interacting cracks are produced by different applied stress fields. In addition, states of propagation (i.e. a two-crack versus one-crack propagation) and array geometries also produce significant differences in damage distribution (Weinberger 1998). Below we discuss the possibility that the distribution and intensity of damage may, in turn, constrain the orientation and relative magnitudes of the stress field acting during en-echelon crack formation.

4.1 *Correlation between observed and simulated damage zones*

In our field example, host-rock (sandstone) deformation manifested by deformation bands (Aydin 1978) around en-echelon dyke segments in Makhtesh Ramon, Israel (Weinberger et al. 1995). The deformation bands are asymmetrically distributed around the dyke plane, forming damage within zones *a*, *b*, and *c*, but are almost absent within zone *d* (Fig. 7; inset). In some cases, the sense of shear in specific locations within these zones can be deduced, and kinematic indicators along the dyke wall suggest that all its segments propagated northward (one-crack propagation). The twist angle of the en echelon array is relatively small (β=5°). For the purpose of correlation between field observations and

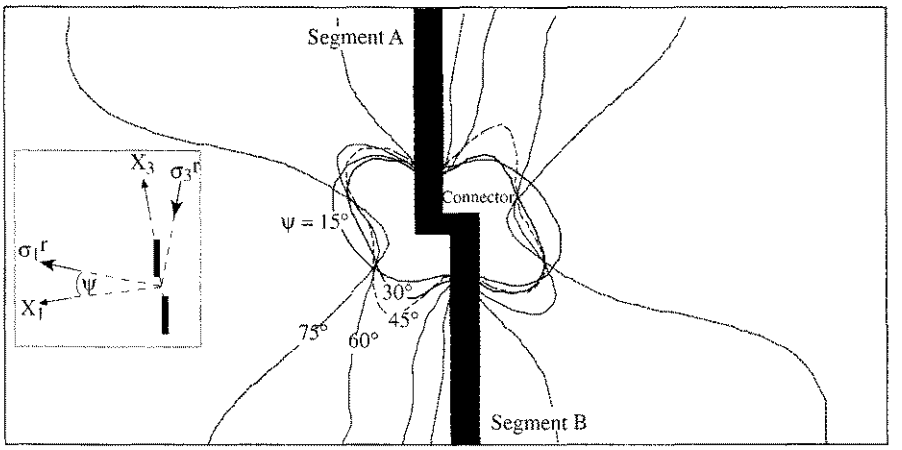

Figure 5. Isodamage lines (i.e. contours of equal magnitude of damage intensity of α=0.02) during segment-connection for variable pairs of (ψ, R). Inset: orientations of the remote principal stresses with respect to the en-echelon cracks in the X_1X_3 plane.

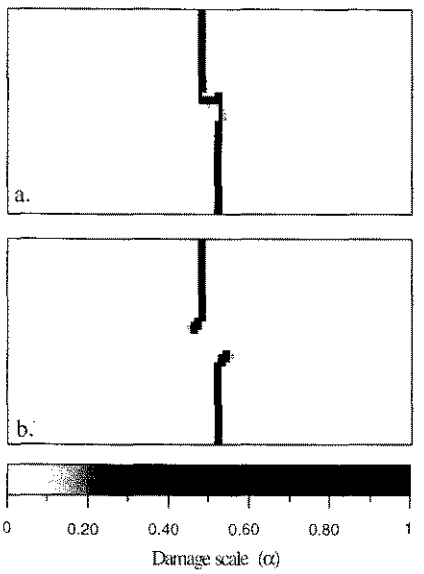

Figure 6. Distributed damage and propagation paths of two en-echelon cracks subjected to effective lithostatic pressure. (a) Induced shear stress for ψ=45°. (b) High magnitude of right-lateral shear stress produces out-of-plane propagation and discontinuity in plan view.

the above simulations, crack density maps of deformation zones around en-echelon dyke segments were prepared by moving a counting square of size 10x10 cm^2 over the deformation zones. Adjacent squares overlapped each other by an area of 5x10 cm^2. The crack density D_f was estimated from the relation:

$$D_f = \sum_{i=1}^{n} L_i^2 / A \qquad (6)$$

where L_i is the length of a particular fracture, and n is the number of fractures within a rectangle area of size A. The data obtained were smoothed by averaging every point with its nearest eight neighbors, and presented in Figure 7a for a particular case study. At present, the scaling between the crack density D_f and the damage intensity α is not already understood. However, the two values should be correlated because both represent fracture processes in the host rock during crack propagation, suggesting that some generalizations can be cautiously made.

A one-crack propagation and β=5° are incorporated in the model setup. Simulations are adjusted until the solutions fulfill two requirements: (1) produce the observed (field) asymmetric distribution of damage, including intense damage within zone a, moderate damage within zones b and c, and minor damage within zone d; (2) produce the observed sense of shear in specific locations around the segments (not shown here). A qualitative comparison between the observed crack-density distribution (D_f) and the damage intensity in a particular simulation is presented in Figure 7. Excluding some discrepancies, the damage zones obtained in the present simulation satisfactorily correlate with the field observations.

4.2 *Inferring the stress state from damage zones around dyke cracks*

The geometry of the model-derived damage zones are consistent with field observations, and thus may constrain the stress state acting during dyke emplacement. In practice, the method outlined above,

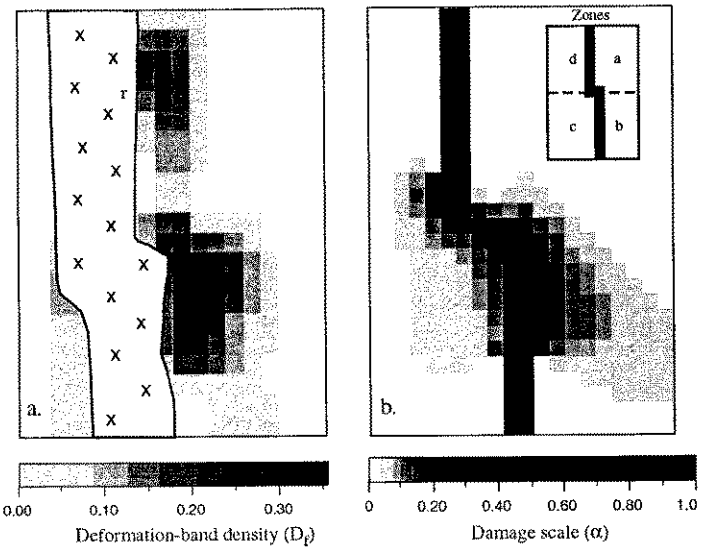

Figure 7. Comparison between field observations and simulated damage zones around two en-echelon dyke segments. (a) Crack (deformation-bands)-density map. (b) Simulated damage zones for (ψ,R)=(45°,22.5) and one-crack propagation. Inset: Definition of zones around connected segments.

whereby a simulation is adjusted to fit the observations, may be used to relate the geometry of the distributed damage around the en-echelon segments to the stress state prevailing during their formation. In the present study, the state of stress simulation that best agrees with the observations is ψ=45° and moderate to high stress ratio R (R~20), respectively. Changes both in the far field (i.e., regional stress field and the stress field associated with a central intrusion) or in the local fields (i.e. heterogeneities such as adjacent structures and bedding interfaces) may contribute to the stress state during dyke emplacement.

5 CONCLUSIONS

1. The geometry of damage zones distributed around en-echelon cracks reflects to the state of stress (ψ, R) acting during propagation, and the geometry of the en-echelon cracks defined by β.
2. The damage model produces different types of crack connections, depending on the initial arrangement of the cracks, mutuality of segment propagation and the stress state.
3. The damage zones yielded by the model satisfactorily correlate with field observations, and may be used to constrain the stress state during formation of en-echelon pressurized cracks.

REFERENCES

Abelson, M., & A. Agnon 1997. Mechanics of oblique spreading and ridge segmentation. *Earth Planet. Sci. Lett.* 148:405-421.

Agnon, A. & V. Lyakhovsky 1995. Damage distribution and localization during dyke intrusion. In G. Baer & A. Heimann (eds), *The physics and chemistry of dykes*: 65-78. Rotterdam:Balkema.

Aydin, A. 1978. Small faults formed as deformation bands in sandstone. *Pure & Appl. Geophys.* 116:913-930.

Barenblatt, G.I. 1962. Mathematical theory of equilibrium cracks in brittle fracture. *Acv. Appl. Mech.* 7:55-129.

Barenblatt, G.I. 1996. *Scaling, self-similarity, and intermediate asymptotic.* Cambridge: Cambridge Univ. Press.

Bazant, Z.P. & L. Cedolin 1991. *Stability of structures: elastic, inelastic, fracture and damage theories.* London:Oxford University Press.

Chai, H. 1993. Observation of deformation and damage at the tip of cracks in adhesive bonds loaded in shear and assessment of a criterion for fracture. *Int. J. Fracture* 60:311-326.

Collins, J. A. 1993. *Failure of Materials in Mechanical Design.* New York:John Wiley.

Cruikshank K.M., G. Zhao & A.M. Johnson 1991. Analysis of minor fractures associated with joints and faulted joints. *J Struct. Geol.* 13:865-886.

Crouch, S. L. & A. M. Starfield 1983. *Boundary element methods in solid mechanics: with applications in rock mechanics and geological*

engineering. London:George Allen & Unwin.

Cundall, P.A. & M. Board 1988. A microcomputer program for modeling large-strain plasticity problems. In C. Swoboda (ed.), *Numerical methods in geomechanics, proc. 6th int. conf. numerical methods in geomechanics, Innsbruck.*: 2101-2108. Rotterdam:Balkhema.

Dugdale, D.S. 1960. Yielding of steel sheets containing slits. *J. Mech. Phys. Solids* 8:100-104.

Huang, W-L., B. Kunin & A. Chudnovsky 1991. Kinematics of damage zone accompanying curved crack. *Int. J. Fracture*. 50:143-152.

Jaeger, J.C. & N.G.W. Cook 1979. *Fundamentals of rock mechanics*. London:Chapman & Hall.

Kachanov, M. 1994. On the concept of damage in creep and in the britt;e-elastic range. *Int. J. Damage Mech.*, 3:329-337.

Lister, J.R., & R.C. Kerr 1991. Fluid mechanical models of crack propagation and their application to magma transport in dikes. *J. Geophys. Res.* 96:10049-10077.

Lockner, D.A., J.D. Byerlee, V. Kuksenko, A.Ponomarev & A. Sidorin 1991. Quasi-static fault growth and shear fracture energy in granite. *Nature* 350:39-42.

Lockner, D.A., D.E. Moore, and Z. Reches 1992. Microcrack interaction leading to shear fracture.. In Tillerson & Wawersik (eds) *Rock mechanics:* 807-816. Rotterdam:Balkema.

Lyakhovsky, V.A. & V.P. Myasnikov 1984. On the behavior of elastic cracked solid. *Phys. Solid Earth* 10:71-75.

Lyakhovsky, V.A. & V.P. Myasnikov 1985. On the behavior of visco-elastic cracked solid. *Phys. Solid Earth* 4:28-35.

Lyakhovsky, V., Y. Podladchikov, and A. Poliakov, Rheological 1993. Model of a fractured solid. *Tectonophysics* 226:187-198.

Lyakhovsky, V., Y. Ben-Zion, & A. Agnon 1997a. Distributed damage, faulting, and friction. *J. Geophys. Res.* 102:27,635-27,649.

Lyakhovsky, V., Z. Reches, R. Weinberger & T.E. Scott 1997b. Non-linear elastic behavior of damaged rocks. *Geophys. J. Int.* 130:157-166.

Meriaux, C., Lister, J. R., Lyakhovsky, V., & Agnon, A. in press. Dyke propagation with distributed damage of the host rock. *Earth Planet. Sci. Lett.*.

Nicholson, R., & D.D. Pollard 1985.Dilation and linkage of echelon cracks. *J. Struc. Geol.* 7:583-590.

Pestman, B.J. & J.G. Munster 1996. An acoustic emission study of damage development and stress - memory effects in sandstone. *Int. J. Rock Mech. Min. Sci.* 33:585-593.

Pollard, D.D., O.H. Muller, & D.R. Dockstader 1975. The form and growth of fingered sheet intrusions. *Geol. Soc. Am. Bull.* 86:351-363.

Pollard, D. D., P. Segall, & P. T. Delaney 1982. Formation and interpretation of dilatant echelon cracks. *Geol. Soc. Am. Bull.* 93:1291-1303.

Poliakov, A., P. Cundall, Y. Podladchikov, & V. Lyakhovsky 1993. An explicit inertial method for the simulation of viscoelastic flow: an evaluation of elastic effects on diapiric flow in two- and three-layers model. In K.E. Runcorn & D. Stone (eds.), *Proceedings of the NATO advanced study institute on dynamic modeling and flow in the earth and planets*: 175-195. Dordrecht: Kluwer.

Reches, Z. & D.A. Lockner 1994. Nucleation and growth of faults in brittle rocks. *J. Geophys. Res.* 99:18159-18173.

Rubin, A. M. 1993. Tensile fracture of rock at high confining pressure: implications for dike propagation, *J. Geophys. Res.* 98:15919-15935.

Valanis, K.C. 1990. A theory of damage in brittle materials. *Eng. Fract. Mech.* 36:403-416.

Weinberger, R., Z.Reches, A. Eidelman & T.S. Scott 1994. Tensile properties of rocks in four-point beam tests under confining pressure. In P. Nelson & S.E. Laubach (eds)*Rock mechanics models and measurements challenges for industry:* 435-442. Rotterdam: Balkema.

Weinberger, R., G. Baer, G. Shamir, & A. Agnon 1995. Deformation bands associated with dyke propagation in porous sandstone, Makhtesh Ramon, Israel. In G. Baer & A. Heimann (eds), *The physics and chemistry of dykes*: 95-112. Rotterdam:Balkema.

Weinberger, R. 1998. Rock deformation associated with dyke emplacement and nonlinear behavior of rocks, *Ph.D thesis, The Hebrew University & report* #GSI/17/98.

Yukutake, H. 1989. Fracturing process of granite inferred from measurements of spatial and temporal variations in velocity during triaxial deformation. *J. Geophys. Res.* 94:15639-15651.

Zietlow, W.K. & J.F. Labuz 1998. Measurement of the intrinistic process zone in rock using acoustic emission. *Int. J. Rock Mech. Min. Sci.* 35:291-299.